Supplementary Information

Probing Side-chain Dynamics in Proteins by NMR Relaxation of Isolated ^{13}C Magnetization Modes in $^{13}CH_3$ Methyl Groups

Vitali Tugarinov,* Alberto Ceccon and G. Marius Clore*

Laboratory of Chemical Physics, National Institute of Diabetes and Digestive and Kidney Diseases, National Institutes of Health, Bethesda, Maryland 20892-0520, USA

Relaxation rates of ^{13}C magnetization modes in a $^{13}CH_3$ spin-system.

Below we provide differential equations that describe the $R_2(C_{\pm})$ and $R_1(C_z)$ relaxation decay processes due to intra-methyl spin interactions within a $^{13}CH_3$ spin-system, calculated using the basis set comprising all the magnetization modes in Eq. 1 of the main text.

R_2 relaxation due to ^{13}C-^{1}H dipolar interactions:

$$\frac{d}{dt}\begin{bmatrix} L_1+L_4 \\ L_2+L_3 \\ L_5+L_6 \\ L_1-L_4 \\ L_2-L_3 \\ L_5-L_6 \end{bmatrix} = -k_{\mathrm{CH}} \left\{ \begin{array}{l} J_{\mathrm{CH}}^{auto}(0) \begin{bmatrix} 1/2 & 0 & 0 & 0 & 0 & 0 \\ 0 & 5/18 & \sqrt{2}/9 & 0 & 0 & 0 \\ 0 & \sqrt{2}/9 & 7/18 & 0 & 0 & 0 \\ 0 & 0 & 0 & 1/2 & 0 & 0 \\ 0 & 0 & 0 & 0 & 5/18 & \sqrt{2}/9 \\ 0 & 0 & 0 & 0 & \sqrt{2}/9 & 7/18 \end{bmatrix} + J_{\mathrm{CH}}^{auto}(\omega_C) \begin{bmatrix} 3/8 & 0 & 0 & 0 & 0 & 0 \\ 0 & 3/8 & 0 & 0 & 0 & 0 \\ 0 & 0 & 3/8 & 0 & 0 & 0 \\ 0 & 0 & 0 & 3/8 & 0 & 0 \\ 0 & 0 & 0 & 0 & 3/8 & 0 \\ 0 & 0 & 0 & 0 & 0 & 3/8 \end{bmatrix} + \\ J_{\mathrm{CH}}^{auto}(\omega_H) \begin{bmatrix} 3/8 & 1/8 & \sqrt{2}/8 & 0 & 0 & 0 \\ 1/8 & 13/24 & \sqrt{2}/24 & 0 & 0 & 0 \\ \sqrt{2}/8 & \sqrt{2}/24 & 7/12 & 0 & 0 & 0 \\ 0 & 0 & 0 & 3/8 & 1/8 & \sqrt{2}/8 \\ 0 & 0 & 0 & 1/8 & 5/24 & -\sqrt{2}/24 \\ 0 & 0 & 0 & \sqrt{2}/8 & -\sqrt{2}/24 & 1/6 \end{bmatrix} + J_{\mathrm{CH}}^{auto}(\omega_C+\omega_H) \begin{bmatrix} 3/4 & 0 & 0 & 0 & 0 & 0 \\ 0 & 3/4 & 0 & 0 & 0 & 0 \\ 0 & 0 & 3/4 & 0 & 0 & 0 \\ 0 & 0 & 0 & 3/4 & 0 & 0 \\ 0 & 0 & 0 & 0 & 3/4 & 0 \\ 0 & 0 & 0 & 0 & 0 & 3/4 \end{bmatrix} \\ + J_{\mathrm{CH}}^{auto}(\omega_H-\omega_C) \begin{bmatrix} 1/8 & 0 & 0 & 0 & 0 & 0 \\ 0 & 1/8 & 0 & 0 & 0 & 0 \\ 0 & 0 & 1/8 & 0 & 0 & 0 \\ 0 & 0 & 0 & 1/8 & 0 & 0 \\ 0 & 0 & 0 & 0 & 1/8 & 0 \\ 0 & 0 & 0 & 0 & 0 & 1/8 \end{bmatrix} \end{array} \right\} \begin{bmatrix} L_1+L_4 \\ L_2+L_3 \\ L_5+L_6 \\ L_1-L_4 \\ L_2-L_3 \\ L_5-L_6 \end{bmatrix}$$

$$-k_{\mathrm{CH}} \left\{ \begin{array}{l} J_{\mathrm{CH}}^{cross}(0) \begin{bmatrix} 1 & 0 & 0 & 0 & 0 & 0 \\ 0 & -1/9 & -\sqrt{2}/9 & 0 & 0 & 0 \\ 0 & -\sqrt{2}/9 & -2/9 & 0 & 0 & 0 \\ 0 & 0 & 0 & 1 & 0 & 0 \\ 0 & 0 & 0 & 0 & -1/9 & -\sqrt{2}/9 \\ 0 & 0 & 0 & 0 & -\sqrt{2}/9 & -2/9 \end{bmatrix} + J_{\mathrm{CH}}^{cross}(\omega_C) \begin{bmatrix} 3/4 & 0 & 0 & 0 & 0 & 0 \\ 0 & -1/4 & 0 & 0 & 0 & 0 \\ 0 & 0 & -1/4 & 0 & 0 & 0 \\ 0 & 0 & 0 & 3/4 & 0 & 0 \\ 0 & 0 & 0 & 0 & -1/4 & 0 \\ 0 & 0 & 0 & 0 & 0 & -1/4 \end{bmatrix} + \\ J_{\mathrm{CH}}^{cross}(\omega_H) \begin{bmatrix} 0 & 1/4 & -\sqrt{2}/8 & 0 & 0 & 0 \\ 1/4 & 5/6 & -\sqrt{2}/24 & 0 & 0 & 0 \\ -\sqrt{2}/8 & -\sqrt{2}/24 & -1/3 & 0 & 0 & 0 \\ 0 & 0 & 0 & 0 & 1/4 & -\sqrt{2}/8 \\ 0 & 0 & 0 & 1/4 & 1/6 & \sqrt{2}/24 \\ 0 & 0 & 0 & -\sqrt{2}/8 & \sqrt{2}/24 & -1/6 \end{bmatrix} + J_{\mathrm{CH}}^{cross}(\omega_C+\omega_H) \begin{bmatrix} 0 & 0 & 0 & 0 & 0 & 0 \\ 0 & 1 & 0 & 0 & 0 & 0 \\ 0 & 0 & -1/2 & 0 & 0 & 0 \\ 0 & 0 & 0 & 0 & 0 & 0 \\ 0 & 0 & 0 & 0 & 1 & 0 \\ 0 & 0 & 0 & 0 & 0 & -1/2 \end{bmatrix} \\ + J_{\mathrm{CH}}^{cross}(\omega_H-\omega_C) \begin{bmatrix} 0 & 0 & 0 & 0 & 0 & 0 \\ 0 & 1/6 & 0 & 0 & 0 & 0 \\ 0 & 0 & -1/12 & 0 & 0 & 0 \\ 0 & 0 & 0 & 0 & 0 & 0 \\ 0 & 0 & 0 & 0 & 1/6 & 0 \\ 0 & 0 & 0 & 0 & 0 & -1/12 \end{bmatrix} \end{array} \right\} \begin{bmatrix} L_1+L_4 \\ L_2+L_3 \\ L_5+L_6 \\ L_1-L_4 \\ L_2-L_3 \\ L_5-L_6 \end{bmatrix}$$

R_1 relaxation due to ^{13}C-^{1}H dipolar interactions:

$$\frac{d}{dt}\begin{bmatrix} L_1+L_4 \\ L_2+L_3 \\ L_5+L_6 \\ L_1-L_4 \\ L_2-L_3 \\ L_5-L_6 \end{bmatrix} = -k_{\mathrm{CH}} \left\{ \begin{aligned} & J_{\mathrm{CH}}^{auto}(0) \begin{bmatrix} 0 & 0 & 0 & 0 & 0 & 0 \\ 0 & 2/9 & -\sqrt{2}/9 & 0 & 0 & 0 \\ 0 & -\sqrt{2}/9 & 1/9 & 0 & 0 & 0 \\ 0 & 0 & 0 & 0 & 0 & 0 \\ 0 & 0 & 0 & 0 & 2/9 & -\sqrt{2}/9 \\ 0 & 0 & 0 & 0 & -\sqrt{2}/9 & 1/9 \end{bmatrix} + J_{\mathrm{CH}}^{auto}(\omega_C) \begin{bmatrix} 3/4 & 0 & 0 & 0 & 0 & 0 \\ 0 & 5/12 & \sqrt{2}/6 & 0 & 0 & 0 \\ 0 & \sqrt{2}/6 & 7/12 & 0 & 0 & 0 \\ 0 & 0 & 0 & 3/4 & 0 & 0 \\ 0 & 0 & 0 & 0 & 5/12 & \sqrt{2}/6 \\ 0 & 0 & 0 & 0 & \sqrt{2}/6 & 7/12 \end{bmatrix} + \\ & J_{\mathrm{CH}}^{auto}(\omega_H) \begin{bmatrix} 3/8 & -1/8 & -\sqrt{2}/8 & 0 & 0 & 0 \\ -1/8 & 5/24 & -\sqrt{2}/24 & 0 & 0 & 0 \\ -\sqrt{2}/8 & -\sqrt{2}/24 & 1/6 & 0 & 0 & 0 \\ 0 & 0 & 0 & 3/8 & -1/8 & -\sqrt{2}/8 \\ 0 & 0 & 0 & -1/8 & 13/24 & \sqrt{2}/24 \\ 0 & 0 & 0 & -\sqrt{2}/8 & \sqrt{2}/24 & 7/12 \end{bmatrix} + J_{\mathrm{CH}}^{auto}(\omega_C+\omega_H) \begin{bmatrix} 3/4 & 1/4 & \sqrt{2}/4 & 0 & 0 & 0 \\ 1/4 & 13/12 & \sqrt{2}/12 & 0 & 0 & 0 \\ \sqrt{2}/4 & \sqrt{2}/12 & 7/6 & 0 & 0 & 0 \\ 0 & 0 & 0 & 3/4 & 1/4 & \sqrt{2}/4 \\ 0 & 0 & 0 & 1/4 & 5/12 & -\sqrt{2}/12 \\ 0 & 0 & 0 & \sqrt{2}/4 & -\sqrt{2}/12 & 1/3 \end{bmatrix} \\ & + J_{\mathrm{CH}}^{auto}(\omega_H-\omega_C) \begin{bmatrix} 1/8 & 1/24 & \sqrt{2}/24 & 0 & 0 & 0 \\ 1/24 & 13/72 & \sqrt{2}/72 & 0 & 0 & 0 \\ \sqrt{2}/24 & \sqrt{2}/72 & 7/36 & 0 & 0 & 0 \\ 0 & 0 & 0 & 1/8 & 1/24 & \sqrt{2}/24 \\ 0 & 0 & 0 & 1/24 & 5/72 & -\sqrt{2}/72 \\ 0 & 0 & 0 & \sqrt{2}/24 & -\sqrt{2}/72 & 1/18 \end{bmatrix} \end{aligned} \right\} \begin{bmatrix} L_1+L_4 \\ L_2+L_3 \\ L_5+L_6 \\ L_1-L_4 \\ L_2-L_3 \\ L_5-L_6 \end{bmatrix}$$

$$-k_{\mathrm{CH}} \left\{ \begin{aligned} & J_{\mathrm{CH}}^{cross}(0) \begin{bmatrix} 0 & 0 & 0 & 0 & 0 & 0 \\ 0 & -2/9 & \sqrt{2}/9 & 0 & 0 & 0 \\ 0 & \sqrt{2}/9 & -1/9 & 0 & 0 & 0 \\ 0 & 0 & 0 & 0 & 0 & 0 \\ 0 & 0 & 0 & 0 & -2/9 & \sqrt{2}/9 \\ 0 & 0 & 0 & 0 & \sqrt{2}/9 & -1/9 \end{bmatrix} + J_{\mathrm{CH}}^{cross}(\omega_C) \begin{bmatrix} 3/2 & 0 & 0 & 0 & 0 & 0 \\ 0 & -1/6 & -\sqrt{2}/6 & 0 & 0 & 0 \\ 0 & -\sqrt{2}/6 & -1/3 & 0 & 0 & 0 \\ 0 & 0 & 0 & 3/2 & 0 & 0 \\ 0 & 0 & 0 & 0 & -1/6 & -\sqrt{2}/6 \\ 0 & 0 & 0 & 0 & -\sqrt{2}/6 & -1/3 \end{bmatrix} + \\ & J_{\mathrm{CH}}^{cross}(\omega_H) \begin{bmatrix} 0 & -1/4 & \sqrt{2}/8 & 0 & 0 & 0 \\ -1/4 & 1/6 & \sqrt{2}/24 & 0 & 0 & 0 \\ \sqrt{2}/8 & \sqrt{2}/24 & -1/6 & 0 & 0 & 0 \\ 0 & 0 & 0 & 0 & -1/4 & \sqrt{2}/8 \\ 0 & 0 & 0 & -1/4 & 5/6 & -\sqrt{2}/24 \\ 0 & 0 & 0 & \sqrt{2}/8 & -\sqrt{2}/24 & -1/3 \end{bmatrix} + J_{\mathrm{CH}}^{cross}(\omega_C+\omega_H) \begin{bmatrix} 0 & 1/2 & -\sqrt{2}/4 & 0 & 0 & 0 \\ 1/2 & 5/3 & -\sqrt{2}/12 & 0 & 0 & 0 \\ -\sqrt{2}/4 & -\sqrt{2}/12 & -2/3 & 0 & 0 & 0 \\ 0 & 0 & 0 & 0 & 1/2 & -\sqrt{2}/4 \\ 0 & 0 & 0 & 1/2 & 1/3 & \sqrt{2}/12 \\ 0 & 0 & 0 & -\sqrt{2}/4 & \sqrt{2}/12 & -1/3 \end{bmatrix} \\ & + J_{\mathrm{CH}}^{cross}(\omega_H-\omega_C) \begin{bmatrix} 0 & 1/12 & -\sqrt{2}/24 & 0 & 0 & 0 \\ 1/12 & 5/18 & -\sqrt{2}/72 & 0 & 0 & 0 \\ -\sqrt{2}/24 & -\sqrt{2}/72 & -1/9 & 0 & 0 & 0 \\ 0 & 0 & 0 & 0 & 1/12 & -\sqrt{2}/24 \\ 0 & 0 & 0 & 1/12 & 1/18 & \sqrt{2}/72 \\ 0 & 0 & 0 & -\sqrt{2}/24 & \sqrt{2}/72 & -1/18 \end{bmatrix} \end{aligned} \right\} \begin{bmatrix} L_1+L_4 \\ L_2+L_3 \\ L_5+L_6 \\ L_1-L_4 \\ L_2-L_3 \\ L_5-L_6 \end{bmatrix}$$

R_1 and R_2 relaxation due to ^{1}H-^{1}H dipolar interactions:

$$\frac{d}{dt}\begin{bmatrix} L_1+L_4 \\ L_2+L_3 \\ L_5+L_6 \\ L_1-L_4 \\ L_2-L_3 \\ L_5-L_6 \end{bmatrix} = -k_{\mathrm{HH}} \left\{ J_{\mathrm{HH}}^{auto}(0) \begin{bmatrix} 0 & 0 & 0 & 0 & 0 & 0 \\ 0 & 1/2 & -\sqrt{2}/4 & 0 & 0 & 0 \\ 0 & -\sqrt{2}/4 & 1/4 & 0 & 0 & 0 \\ 0 & 0 & 0 & 0 & 0 & 0 \\ 0 & 0 & 0 & 0 & 1/2 & -\sqrt{2}/4 \\ 0 & 0 & 0 & 0 & -\sqrt{2}/4 & 1/4 \end{bmatrix} + J_{\mathrm{HH}}^{auto}(\omega_H) \begin{bmatrix} 3/4 & -1/2 & -\sqrt{2}/8 & 0 & 0 & 0 \\ -1/2 & 5/4 & -3\sqrt{2}/8 & 0 & 0 & 0 \\ -\sqrt{2}/8 & -3\sqrt{2}/8 & 1/2 & 0 & 0 & 0 \\ 0 & 0 & 0 & 3/4 & -1/2 & -\sqrt{2}/8 \\ 0 & 0 & 0 & -1/2 & 5/4 & 3\sqrt{2}/8 \\ 0 & 0 & 0 & -\sqrt{2}/8 & 3\sqrt{2}/8 & 1/2 \end{bmatrix} + J_{\mathrm{HH}}^{auto}(2\omega_H) \begin{bmatrix} 3/2 & -1/2 & -\sqrt{2}/2 & 0 & 0 & 0 \\ -1/2 & 1/2 & 0 & 0 & 0 & 0 \\ -\sqrt{2}/2 & 0 & 1/2 & 0 & 0 & 0 \\ 0 & 0 & 0 & 3/2 & 1/2 & \sqrt{2}/2 \\ 0 & 0 & 0 & 1/2 & 1/2 & 0 \\ 0 & 0 & 0 & \sqrt{2}/2 & 0 & 1/2 \end{bmatrix} \right\} \begin{bmatrix} L_1+L_4 \\ L_2+L_3 \\ L_5+L_6 \\ L_1-L_4 \\ L_2-L_3 \\ L_5-L_6 \end{bmatrix}$$

$$-k_{\mathrm{HH}} \left\{ J_{\mathrm{HH}}^{cross}(0) \begin{bmatrix} 0 & 0 & 0 & 0 & 0 & 0 \\ 0 & -1/2 & \sqrt{2}/4 & 0 & 0 & 0 \\ 0 & \sqrt{2}/4 & -1/4 & 0 & 0 & 0 \\ 0 & 0 & 0 & 0 & 0 & 0 \\ 0 & 0 & 0 & 0 & -1/2 & \sqrt{2}/4 \\ 0 & 0 & 0 & 0 & \sqrt{2}/4 & -1/4 \end{bmatrix} + J_{\mathrm{HH}}^{cross}(\omega_H) \begin{bmatrix} 3/4 & -1 & \sqrt{2}/8 & 0 & 0 & 0 \\ -1 & 1/4 & 3\sqrt{2}/8 & 0 & 0 & 0 \\ \sqrt{2}/8 & 3\sqrt{2}/8 & -1/2 & 0 & 0 & 0 \\ 0 & 0 & 0 & 3/4 & -1 & \sqrt{2}/8 \\ 0 & 0 & 0 & -1 & 1/4 & -3\sqrt{2}/8 \\ 0 & 0 & 0 & \sqrt{2}/8 & -3\sqrt{2}/8 & -1/2 \end{bmatrix} + J_{\mathrm{HH}}^{cross}(2\omega_H) \begin{bmatrix} 0 & -1 & \sqrt{2}/2 & 0 & 0 & 0 \\ -1 & 1 & 0 & 0 & 0 & 0 \\ \sqrt{2}/2 & 0 & -1/2 & 0 & 0 & 0 \\ 0 & 0 & 0 & 0 & 1 & -\sqrt{2}/2 \\ 0 & 0 & 0 & 1 & 1 & 0 \\ 0 & 0 & 0 & -\sqrt{2}/2 & 0 & -1/2 \end{bmatrix} \right\} \begin{bmatrix} L_1+L_4 \\ L_2+L_3 \\ L_5+L_6 \\ L_1-L_4 \\ L_2-L_3 \\ L_5-L_6 \end{bmatrix}$$

where $k_{\mathrm{CH}} = \left(\frac{\mu_0}{4\pi}\right)^2 \frac{6\hbar^2\gamma_{\mathrm{H}}^2\gamma_{\mathrm{C}}^2\tau_C}{r_{\mathrm{CH}}^6}$; $k_{\mathrm{HH}} = \left(\frac{\mu_0}{4\pi}\right)^2 \frac{6\hbar^2\gamma_{\mathrm{H}}^4\tau_C}{r_{\mathrm{HH}}^6}$; μ_0 is the vacuum permeability constant, γ_{H} and γ_{C}, gyromagnetic ratios of proton and carbon spins, respectively; r_{HH} and r_{CH}, ^{1}H-^{1}H and ^{13}C-^{1}H internuclear distances in a methyl group, and τ_C the global molecular rotational correlation time (assumed isotropic). Auto- and cross-correlated relaxation spectral density functions $J(\omega)$ are labelled by the superscripts 'auto' and 'cross', respectively, while the subscripts denote the type of interaction ('HH' for ^{1}H-^{1}H interactions, and 'CH' for ^{13}C-^{1}H interactions. The spectral density function used throughout this work has the following 'model-free'[1,2] form,[3]

$$J_{\mu\nu}(\omega) = \frac{1}{5}\left\{ S^2_{axis} S_{axis,\mu} S_{axis,\nu} \frac{\tau_C}{1+(\omega\tau_C)^2} + \left[P_2(\cos\theta_{\mu,\nu}) - S^2_{axis} S_{axis,\mu} S_{axis,\nu} \right] \frac{\tau_e}{1+(\omega\tau_e)^2} \right\} \quad \text{(S1)}$$

where $\tau_e^{-1} = \tau_C^{-1} + \tau_f^{-1}$; the indices '$\mu$' and '$\nu$' denote the type of interaction ($\mu = \nu$ and $\mu \neq \nu$ for 'auto'- and 'cross'-correlated spectral density functions, respectively); $P_2(\cos(x)) = (1/2)[3\cos^2(x) - 1]$, $S_{axis,a} = P_2(\cos(\theta_{axis,a}))$, and $\theta_{axis,a}$ is the angle subtended by the methyl symmetry axis and vector a connecting a pair of spins. For example, for ^{13}C-^{1}H interactions, $S_{axis,a} = P_2(\cos(\theta_{axis,CH})) = -1/3$, while for ^{1}H-^{1}H interactions, $S_{axis,a} = P_2(\cos(\theta_{axis,HH})) = -1/2$.

In addition, all the ^{13}C magnetization modes relax due to methyl ^{13}C chemical shift anisotropy (CSA), with the corresponding rates given by,

$$R_{2,\text{csa}} = k_{\text{csa}}\{ (2/3)J_{\text{csa}}(0) + (1/2)J_{\text{csa}}(\omega_C)\} \quad \text{(S2.1)}$$

$$R_{1,\text{csa}} = k_{\text{csa}} J_{\text{csa}}(\omega_C) \quad \text{(S2.2)}$$

where

$k_{\text{csa}} = \frac{1}{3}(\omega_C \Delta_C)^2$, Δ_C is methyl ^{13}C CSA, and

$$J_{\text{csa}}(\omega) = \frac{2}{5}\left\{ S^2_{axis} \frac{\tau_C}{1+(\omega\tau_C)^2} + (1 - S^2_{axis}) \frac{\tau_e}{1+(\omega\tau_e)^2} \right\}, \quad \text{(S2.3)}$$

while no cross-relaxation between ^{13}C magnetization modes occurs due to this mechanism.

Earlier, Kay and Bull[4] derived relaxation matrices for transverse ^{13}C relaxation in AX_3($^{13}CH_3$) spin-systems albeit using a slightly different basis set. No secular approximation has been used in the derivation of the relaxation matrices above (the modes can cross-relax even if they have different precession frequencies). Note that methyl-^{13}C CSA/^{13}C-^{1}H dipolar cross correlated relaxation is the only mechanism by which the in-phase modes can cross-relax with the anti-phase modes in the basis of Eq. 1 (main text). We did not include these cross-correlations in the calculations above as they are eliminated by application of ^{1}H 180° pulses during relaxation delays in the experiments described in this work (hence, the block-diagonal structure of the relaxation matrices above). As long as (1) one of the ^{13}C

magnetization modes is isolated before the relaxation period, and (2) not excessively long relaxation delays are used in relaxation measurements, the decay of each of ^{13}C modes is single-exponential to a good approximation. Below we list the relaxation rates of the ^{13}C magnetization modes that are used for derivation of methyl axis dynamics parameters in this work, in the 'single-exponential' limit (preserving only the diagonal elements of the relaxation matrices above).

($L_5 + L_6$) mode:

$$\begin{aligned} R_2 = {} & k_{\mathrm{CH}} \{ (7/18)\ J^{auto}_{\mathrm{CH}}(0) - (2/9)\ J^{cross}_{\mathrm{CH}}(0) + (3/8)\ J^{auto}_{\mathrm{CH}}(\omega_C) - (1/4)\ J^{cross}_{\mathrm{CH}}(\omega_C) + \\ & (3/4) J^{auto}_{\mathrm{CH}}(\omega_C + \omega_H) - (1/2) J^{cross}_{\mathrm{CH}}(\omega_C + \omega_H) + (1/8) J^{auto}_{\mathrm{CH}}(\omega_H - \omega_C) - (1/12) J^{cross}_{\mathrm{CH}}(\omega_H - \omega_C) + \\ & (7/12) J^{auto}_{\mathrm{CH}}(\omega_H) - (1/3) J^{cross}_{\mathrm{CH}}(\omega_H) \} + \\ & k_{\mathrm{HH}} \{ (1/4)\ J^{auto}_{\mathrm{HH}}(0) - (1/4) J^{cross}_{\mathrm{HH}}(0) + (1/2) J^{auto}_{\mathrm{HH}}(\omega_H) - (1/2) J^{cross}_{\mathrm{HH}}(\omega_H) + \\ & (1/2) J^{auto}_{\mathrm{HH}}(2\omega_H) - (1/2) J^{cross}_{\mathrm{HH}}(2\omega_H) \} + \\ & k_{\mathrm{csa}} \{ (2/3) J_{\mathrm{csa}}(0) + (1/2) J_{\mathrm{csa}}(\omega_C) \}; \end{aligned} \tag{S3.1}$$

$$\begin{aligned} R_1 = {} & k_{\mathrm{CH}} \{ (1/9)\ J^{auto}_{\mathrm{CH}}(0) - (1/9)\ J^{cross}_{\mathrm{CH}}(0) + (7/12)\ J^{auto}_{\mathrm{CH}}(\omega_C) - (1/3)\ J^{cross}_{\mathrm{CH}}(\omega_C) + \\ & (7/6) J^{auto}_{\mathrm{CH}}(\omega_C + \omega_H) - (2/3) J^{cross}_{\mathrm{CH}}(\omega_C + \omega_H) + (7/36) J^{auto}_{\mathrm{CH}}(\omega_H - \omega_C) - (1/9) J^{cross}_{\mathrm{CH}}(\omega_H - \omega_C) + \\ & (1/6) J^{auto}_{\mathrm{CH}}(\omega_H) - (1/6) J^{cross}_{\mathrm{CH}}(\omega_H) \} + \\ & k_{\mathrm{HH}} \{ (1/4)\ J^{auto}_{\mathrm{HH}}(0) - (1/4) J^{cross}_{\mathrm{HH}}(0) + (1/2) J^{auto}_{\mathrm{HH}}(\omega_H) - (1/2) J^{cross}_{\mathrm{HH}}(\omega_H) + \\ & (1/2) J^{auto}_{\mathrm{HH}}(2\omega_H) - (1/2) J^{cross}_{\mathrm{HH}}(2\omega_H) \} + \\ & k_{\mathrm{csa}}\ J_{\mathrm{csa}}(\omega_C); \end{aligned} \tag{S3.2}$$

($L_1 \pm L_4$) modes:

$$\begin{aligned} R_2 = {} & k_{\mathrm{CH}} \{ (1/2)\ J^{auto}_{\mathrm{CH}}(0) + J^{cross}_{\mathrm{CH}}(0) + (3/8)\ J^{auto}_{\mathrm{CH}}(\omega_C) + (3/4)\ J^{cross}_{\mathrm{CH}}(\omega_C) + \\ & (3/4) J^{auto}_{\mathrm{CH}}(\omega_C + \omega_H) + (1/8) J^{auto}_{\mathrm{CH}}(\omega_H - \omega_C) + (3/8) J^{auto}_{\mathrm{CH}}(\omega_H) \} + \\ & k_{\mathrm{HH}} \{ (3/4) J^{auto}_{\mathrm{HH}}(\omega_H) + (3/4) J^{cross}_{\mathrm{HH}}(\omega_H) + (3/2) J^{auto}_{\mathrm{HH}}(2\omega_H) \} + \\ & k_{\mathrm{csa}} \{ (2/3) J_{\mathrm{csa}}(0) + (1/2) J_{\mathrm{csa}}(\omega_C) \} + k^{ext}_{\mathrm{HH}}; \end{aligned} \tag{S4.1}$$

$$\begin{aligned} R_1 = {} & k_{\mathrm{CH}} \{ (3/4)\ J^{auto}_{\mathrm{CH}}(\omega_C) + (3/2)\ J^{cross}_{\mathrm{CH}}(\omega_C) + \\ & (3/4) J^{auto}_{\mathrm{CH}}(\omega_C + \omega_H) + (1/8) J^{auto}_{\mathrm{CH}}(\omega_H - \omega_C) + (3/8) J^{auto}_{\mathrm{CH}}(\omega_H) \} + \\ & k_{\mathrm{HH}} \{ (3/4) J^{auto}_{\mathrm{HH}}(\omega_H) + (3/4) J^{cross}_{\mathrm{HH}}(\omega_H) + (3/2) J^{auto}_{\mathrm{HH}}(2\omega_H) \} + \\ & k_{\mathrm{csa}}\ J_{\mathrm{csa}}(\omega_C) + k^{ext}_{\mathrm{HH}}; \end{aligned} \tag{S4.2}$$

where $k_{\mathrm{HH}}^{ext} = \left(\frac{3}{20}\right)\left(\frac{\mu_0}{4\pi}\right)^2 \sum_{ext} \frac{6\hbar^2\gamma_{\mathrm{H}}^4\tau_C}{r_{hhext}^6}$ (see main text).

The differences Δ between R_2/R_1 of the $(L_2 - L_3)$ and $(L_2 + L_3)$ modes (see also Eq. 2 of the main text) are described by,

$$\Delta R_2 = R_{2,(L2-L3)} - R_{2,(L2+L3)} = (8/3)\,k_{\mathrm{HH}}^{ext} - k_{\mathrm{CH}}\{(1/3)\,J_{\mathrm{CH}}^{auto}(\omega_H) + (2/3)\,J_{\mathrm{CH}}^{cross}(\omega_H)\} \approx (8/3)\,k_{\mathrm{HH}}^{ext} \qquad \text{(S5.1)}$$

and

$$\begin{aligned}\Delta R_1 = R_{1,(L2-L3)} - R_{1,(L2+L3)} = (8/3)\,k_{\mathrm{HH}}^{ext} + k_{\mathrm{CH}}\{&(1/3)\,J_{\mathrm{CH}}^{auto}(\omega_H) + (2/3)\,J_{\mathrm{CH}}^{cross}(\omega_H) - \\ &(2/3)\,J_{\mathrm{CH}}^{auto}(\omega_C+\omega_H) - (4/3)\,J_{\mathrm{CH}}^{cross}(\omega_C+\omega_H) - \\ &(1/9)\,J_{\mathrm{CH}}^{auto}(\omega_H-\omega_C) - (2/9)\,J_{\mathrm{CH}}^{cross}(\omega_H-\omega_C)\} \approx (8/3)\,k_{\mathrm{HH}}^{ext}\end{aligned} \qquad \text{(S5.2)}$$

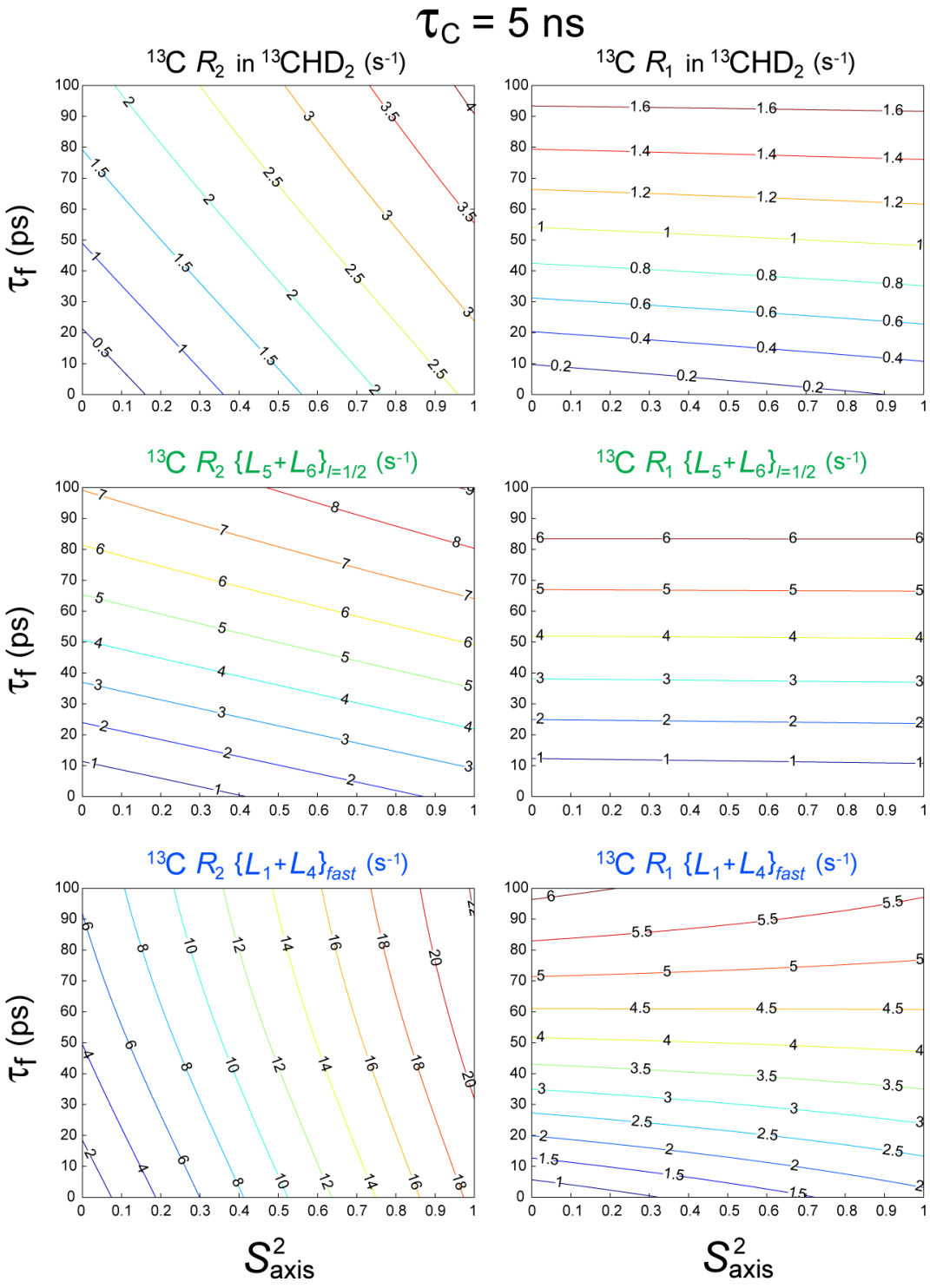

Figure S1. Contour plots of R_2 (left column; s^{-1}) and R_1 (right column; s^{-1}) relaxation rates of ^{13}C nuclei in $^{13}CHD_2$ methyl groups (upper row), the (L_5 + L_6) magnetization mode (I = ½ manifold; middle row), and the (L_1 + L_4) magnetization mode (bottom row) calculated as a function of S^2_{axis} (x-axis) and τ_f (y-axis; ps) for the global correlation time τ_C = 5 ns. Calculations were performed using the parameters of methyl geometry listed in 'Materials and Methods' section below. The rates of the (L_1 + L_4) mode were calculated assuming the distance to a single external proton spin, r_{hhext} = 3.0 Å.

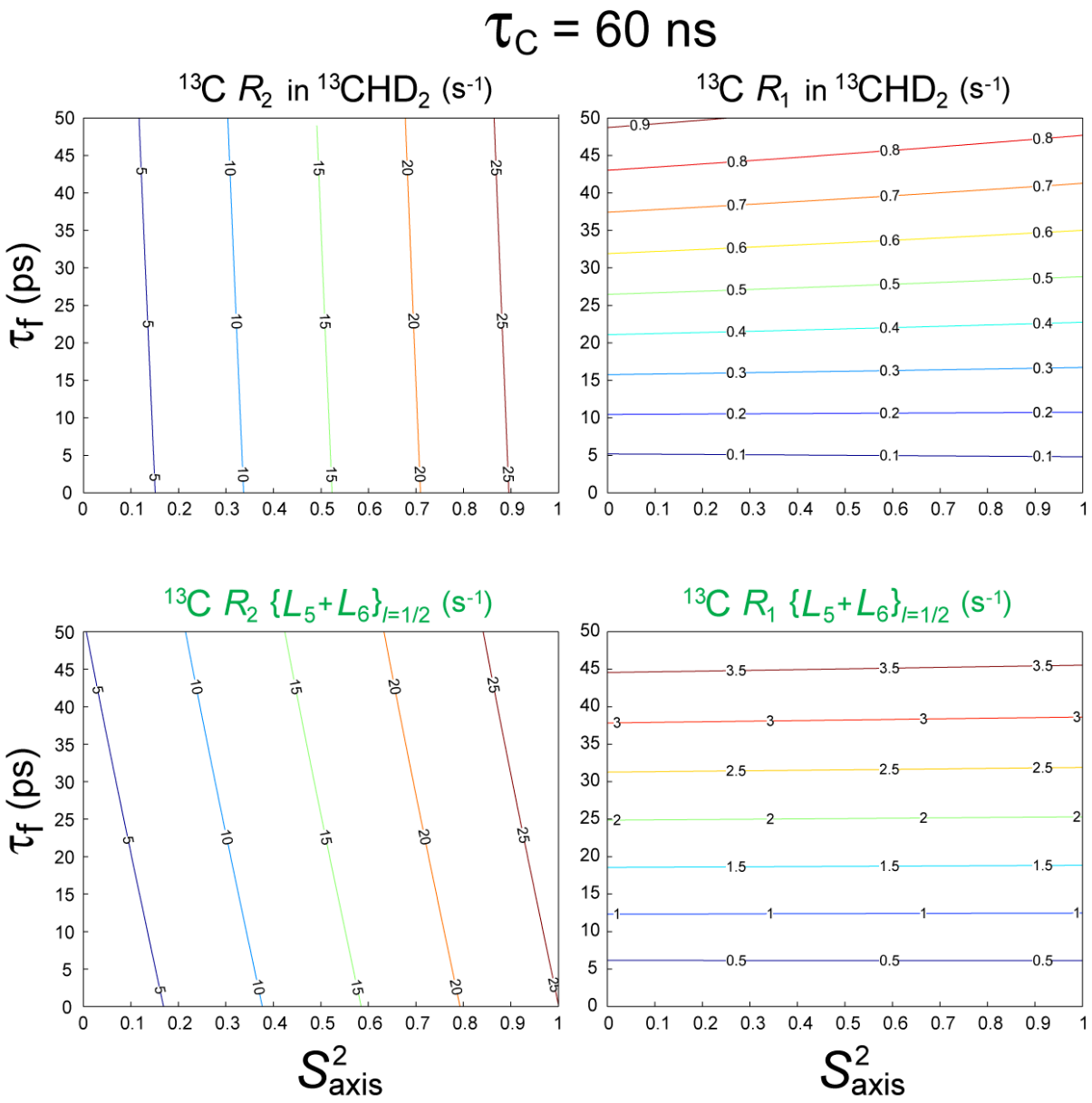

Figure S2. Contour plots of R_2 (left column; s^{-1}) and R_1 (right column; s^{-1}) relaxation rates of ^{13}C nuclei in $^{13}CHD_2$ methyl groups (upper row), and the (L_5 + L_6) magnetization mode (I = 1/2 manifold; bottom row), calculated as a function of S^2_{axis} (x-axis) and τ_f (y-axis; ps) for the global correlation time τ_C = 60 ns. Calculations were performed using the parameters of methyl geometry listed in the 'Materials and Methods' section.

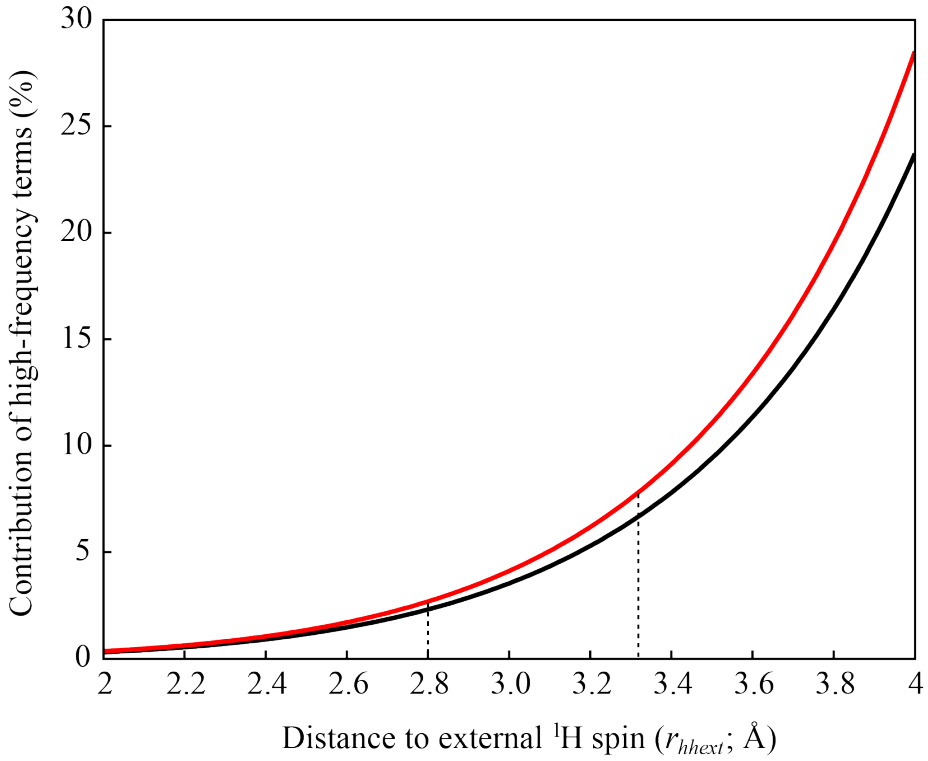

Figure S3. Plot showing the absolute magnitude of contributions of high frequency ($\omega > 0$) terms (in %; *y*-axis) to the differences Δ for R_2 (black curve, Eq. S5.1) and R_1 (red curve, Eq. S5.2) relaxation rates, plotted as a function of the distance to a single external ^{1}H spin (r_{hhext}, in Å; *y*-axis) for ubiquitin at 25 ºC (τ_C = 5 ns). Calculations were performed using a standard set of average methyl axis dynamics parameters: S^2_{axis} = 0.6, and τ_f = 40 ps; the form of the spectral density function is given by Eq. S1; the parameters of methyl geometry are listed in the 'Materials and Methods' section of the SI; and the ^{1}H spectrometer frequency is 600 MHz. Approximate distances to the external ^{1}H spin corresponding to the average (2.1 s^{-1}) and minimal (0.9 s^{-1}) values of Δ measured for ubiquitin at 25 ºC (r_{hhext} = 2.8 Å and 3.3 Å, respectively) are indicated by dashed vertical lines. Note that smaller contributions of high-frequency terms to Δ for R_2/R_1 rates are expected at lower temperatures (higher τ_C values).

Optimization of flip-angles in the pulse schemes of Figures 5 and 6.

The density matrix describing the state of the magnetization in a $^{13}CH_3$ spin-system can be represented as a tensor product, $C \otimes \rho$, where $C \in \{C_x, C_y, C_z, E\}$, C_l is a ^{13}C spin operator, E is the 2x2 identity matrix, and ρ describes the state of ^1H magnetization. The latter is constructed from a basis set of 8 ^1H eigenstates $|n\rangle$ formed by linear combinations of $|i,j,k\rangle$ ($i,j,k \in \{\alpha,\beta\}$) (see Fig. 1; main text). Further, the density matrix ρ and ^1H RF pulse operators can be separated into two parts corresponding to the $I = 3/2$ ($\rho^{3/2}$) and $I = 1/2$ ($\rho^{1/2}$) manifolds, as they evolve independently of each other under the effect of RF field. Here, we concentrate on the transformations of the matrix $\rho^{3/2}$, as $\rho^{1/2}$ is 'taken out of the picture' by selection of the fast relaxing (outer) ^1H transitions at the start of the schemes in Figs. 5 and 6, keeping in mind that the state of the full (8x8) density matrix describing the magnetization of the $I = 3/2$ manifold, can be obtained by the tensor product above.

The scheme for isolation of the ($L_1 \pm L_4$) magnetization mode in Fig. 5 (main text). Following isolation of the fast-relaxing (outer) ^1H transitions (prior to the ^1H_y pulse with flip-angle β shown in blue in Fig. 5), the density matrix is given by,

$$\rho_F^{3/2} = \begin{bmatrix} 0 & \sqrt{3}/2 & 0 & 0 \\ \sqrt{3}/2 & 0 & 0 & 0 \\ 0 & 0 & 0 & \sqrt{3}/2 \\ 0 & 0 & \sqrt{3}/2 & 0 \end{bmatrix} \tag{S6}$$

Using the procedures of analytical matrix exponentiation described previously,[5] we can express the density matrix after the ^1H_y pulse with flip-angle β and the subsequent pulsed field gradient (g′; Fig. 5) as,

$$\rho^{3/2}(\beta) = \frac{1}{4}\begin{bmatrix} -3\sin\beta(\cos^2\beta+1) & 0 & 0 & 0 \\ 0 & 3\sin\beta(3\cos^2\beta-1) & 0 & 0 \\ 0 & 0 & -3\sin\beta(3\cos^2\beta-1) & 0 \\ 0 & 0 & 0 & 3\sin\beta(\cos^2\beta+1) \end{bmatrix} \tag{S7}$$

where only diagonal elements are retained after the pulsed field gradient. Clearly, when $\beta = \cos^{-1}(1/\sqrt{3}) = 54.7°$ ('magic' angle), only the outer ^{1}H states (elements [1,1] and [4,4] of the matrix in Eq. S7) are polarized.

The scheme for isolation of the ($L_2 \pm L_3$) magnetization mode in Fig. 6 (main text). Following the pulsed-field gradient g10 in the scheme of Fig. 6 (prior to the ^1H_y pulse with flip-angle γ shown in red), the signal can be described to within a multiplicative factor by a density matrix given by,

$$\rho_S^{3/2} = \begin{bmatrix} 0 & 0 & 0 & 0 \\ 0 & 1 & 0 & 0 \\ 0 & 0 & -1 & 0 \\ 0 & 0 & 0 & 0 \end{bmatrix} \tag{S8}$$

After the application of the ^1H_y pulse with flip-angle γ and the cycling of its phase ($\phi 6$) with concomitant inversion of the receiver phase, the density matrix takes the form,

$$\rho^{3/2}(\gamma) = \frac{1}{4}\begin{bmatrix} 0 & -\sqrt{3}\sin\gamma(3\cos^2\gamma - 1) & 0 & -\sin^3\gamma \\ -\sqrt{3}\sin\gamma(3\cos^2\gamma - 1) & 0 & \sin\gamma(8 - 9\sin^2\gamma) & 0 \\ 0 & \sin\gamma(8 - 9\sin^2\gamma) & 0 & -\sqrt{3}\sin\gamma(3\cos^2\gamma - 1) \\ -\sin^3\gamma & 0 & -\sqrt{3}\sin\gamma(3\cos^2\gamma - 1) & 0 \end{bmatrix} \tag{S9}$$

We seek to maximize the slow-relaxing part of the magnetization (elements [2,3] and [3,2] of the matrix in Eq. S9) in the rest of the experiment (t_1 and t_2 acquisition periods). Differentiating these elements with respect to γ, yields the optimal value, $\gamma_{opt} = \sin^{-1}(\sqrt{8/27}) = 32.98°$. Note that the fast relaxing ^{1}H magnetization (elements [1,2], [2,1] and [3,4], [4,3] of the matrix in Eq. S9) has to be eliminated subsequently, as for $\gamma = \gamma_{opt}$, this magnetization would generate a signal of opposite sign (that would partially cancel the signal of interest).

Materials and Methods

NMR Samples. Two samples of ubiquitin were used in this work: 1) a {U-[^{15}N,^{2}H]; Ileδ1-[^{13}CH$_3$]; Leu,Val-[^{13}CH$_3$,^{12}CD$_3$]}-labeled, and 2) a {U-[^{15}N,^{2}H]; Ileδ1-[^{13}CHD$_2$]; Leu,Val-[^{13}CHD$_2$,^{12}CD$_3$]}-labeled one. The samples were expressed and purified as described previously[6] using appropriate α-keto-acid precursors for generation of methyl isotopomers of ^{13}CH$_3$ or ^{13}CHD$_2$ variety.[7] In both samples, the concentration of ubiquitin was 1.3 mM in a buffer comprising 99.9% D_2O, 20 mM sodium phosphate, pH 6.5 (uncorrected), and 50 mM NaCl. The samples of {U-[^{15}N,^{2}H]; Ileδ1-[^{13}CH$_3$]}-labeled and {U-[^{15}N,^{2}H]; Ileδ1-[^{13}CHD$_2$]}-labeled Malate Synthase G (MSG) were expressed and purified as described previously.[8,9] Both MSG samples were dissolved in a buffer comprising 99.9% D_2O, 25 mM sodium phosphate (pH 7.0; uncorrected) and 5 mM $MgCl_2$.

The concentration of the {U-[^{15}N,^{2}H]; Ileδ1-[^{13}CHD$_2$]}-labeled MSG sample was 0.5 mM, while the {U-[^{15}N,^{2}H]; Ileδ1-[^{13}CH$_3$]}-labeled MSG was studied at two concentrations - 0.5 mM and 1.1 mM. Using a procedure described in detail previously,[9,10] we established the values of global rotational correlation time τ_C (assumed isotropic in this study) of 46 ns and 64 ns for the 0.5 mM and 1.1 mM, samples, respectively, reflecting a notable viscosity (and hence τ_C) dependence of MSG samples on protein concentration.[9,10] Practically identical correlations between the ^{13}CH$_3$- and ^{13}CHD$_2$-derived methyl axis dynamics parameters [S^2_{axis}; τ_f] were obtained for the two sample concentrations. Figure 4 of the main text shows the correlations obtained for a 0.5 mM sample.

NMR Spectroscopy. All spectra were recorded on a 600 MHz, AVANCE HD Bruker spectrometer equipped with a triple-axis (x, y, z) gradient cryogenic probe and were processed and analyzed using the NMRPipe/NMRDraw suite of programs and associated software.[11] Each of the data sets acquired with the pulse-schemes in Figs. 2, 5 and 6 comprised [96, 512] complex points in [^{13}C(t_1), ^{1}H(t_2)] dimensions translating to acquisition times of [32 ms, 64 ms] and [64 ms, 64 ms] for ILV-{^{13}CH$_3$}-labeled ubiquitin (at both temperatures) and Ileδ1-{^{13}CH$_3$}-labeled MSG, respectively. Typically, 16 and 32 scans per FID were used for ubiquitin and MSG samples, respectively, with inter-scan relaxation delay of 1.5 sec. leading to net acquisition times of ~1.4 and ~2.9 hr. per 2D spectrum for the two proteins, respectively (note that experiments in Figs. 5 and 6 were not acquired for MSG). In all experiments, 2D data sets were recorded as a function of a parametrically varied relaxation delay, T. The following sets of delays T used for relaxation measurements of ^{13}C magnetization modes in ILV-{^{13}CH$_3$}-ubiquitin, ($L_5 + L_6$) $R_{1\rho}$: (0.2, 40, 80, 120, 160, 200) ms, and (0.2, 25, 50, 75, 100, 120) ms at 25 and 5 °C, respectively; ($L_5 + L_6$) R_1: (0, 60, 120, 180, 240, 300) ms, and (0, 50, 100, 150, 200, 250) ms at 25 and 5 °C, respectively; ($L_1 \pm L_4$)

R_2 ('free-precession'): (0, 12, 24, 36, 48, 60) ms, and (0, 6, 12, 18, 24, 30) ms at 25 and 5 °C, respectively; ($L_1 + L_4$) R_1: (0, 40, 80, 120, 160, 200) ms at both temperatures; ($L_2 + L_3$) $R_{1\rho}$: (0.1, 40, 80, 120, 160, 200) ms, and (0.1, 20, 40, 60, 80, 100) ms at 25 and 5 °C, respectively; ($L_2 + L_3$) R_1: (0, 40, 80, 120, 160, 200) ms, and (0, 30, 60, 90, 120, 150) ms at 25 and 5 °C, respectively; ($L_2 - L_3$) $R_{1\rho}$: (0.1, 20, 40, 60, 80, 100) ms, and (0.1, 10, 20, 30, 40, 50) ms at 25 and 5 °C, respectively; and ($L_2 - L_3$) R_1: (0, 30, 60, 90, 120, 150) ms, and (0, 15, 30, 45, 60, 75) ms at 25 and 5 °C, respectively. Delays T used in the measurements of ($L_5 + L_6$) $R_{1\rho}$ and R_1 in Ileδ1-{$^{13}CH_3$}-MSG (37 °C) were (0.2, 15, 30, 45, 60, 80) ms, and (0, 0.2, 0.4, 0.6, 0.8, 1.0) sec, respectively.

It is worth noting that experiments designed for relaxation measurements of the ^{13}C magnetization modes belonging to the $I = 3/2$ manifold (Figs. 5 and 6) are very sensitive to imperfections of the ^1H 180° pulses applied during relaxation delays T in order to eliminate contributions of methyl-^{13}C CSA/^{13}C-^1H dipolar cross correlated relaxation to the measured rates. Even slight deviations of these pulses from ideality can inter-convert the ^{13}C magnetization modes of the $I = 3/2$ manifold. Therefore, extreme care has to be exercised in optimization of these pulses and their phase-cycling as described in the captions to Figs. 5 and 6 of the main text. Simulations show that anti-phase ^{13}C magnetization modes (such as, for example, $L_2 - L_3$) are by far more sensitive to these imperfections. In this regard, we note that relaxation decays obtained in the measurements of the ($L_2 - L_3$) and ($L_1 \pm L_4$) modes performed *without* application of ^1H 180° pulses during delays T altogether, can be fitted to a function $A\exp(-RT)\cosh(\eta T)$, where R is the corresponding relaxation rate and η, the cross-correlated relaxation rate, providing results very similar to those reported in the main text.

The measurements of ^{13}C R_2/R_1 relaxation rates in $^{13}CHD_2$-methyl-labeled samples were performed as described previously[9] (see Figure S1 in SI of ref. 9 for the pulse-scheme). Each of the data sets acquired on [$^{13}CHD_2$]-labeled samples comprised [96, 512] complex points in [$^{13}C(t_1)$, $^1H(t_2)$] dimensions translating to acquisition times of [32 ms, 64 ms] and [64 ms, 64 ms] for ILV-{$^{13}CHD_2$}-labeled ubiquitin (at both temperatures) and Ileδ1-{$^{13}CHD_2$}-labeled MSG, respectively. Typically, 16 and 32 scans per FID were used for {$^{13}CHD_2$}-labeled samples of ubiquitin and MSG, respectively, with inter-scan relaxation delay of 2.5 sec leading to net acquisition times of ~2.2 and ~4.5 hr. (for $T = 0$) for the two samples, respectively. ^{13}C $R_{1\rho}$ rates in $^{13}CHD_2$ methyls of ubiquitin were measured using relaxation delays T of (4, 50, 100, 150, 200, 250, 300) ms and (4, 40, 80, 120, 160, 200, 240) ms at 25 and 5 °C, respectively, while the delays T of (0.04, 0.2, 0.4, 0.6, 0.8, 1.0, 1.2) sec and (0.04, 0.15, 0.3, 0.45, 0.6, 0.8, 1.0) sec were used for R_1 measurements at 25 and 5 °C, respectively. ^{13}C $R_{1\rho}$ and R_1 rates in $^{13}CHD_2$ groups of MSG were measured using relaxation delays T of (0.2, 10, 20, 30, 40, 50, 60) ms and (0.04, 0.5, 1.0, 1.5, 2.0, 2.5, 3.0) sec, respectively.

All ^{13}C $R_{1\rho}$ measurements (for methyl isotopomers of both types) employed 2.0-kHz spin-lock fields. Errors in relaxation rates were estimated on the basis of the noise floor of the data sets. Average ^{13}C R_2 rates of 2.25 and 4.54 s^{-1} were obtained for ILV-{$^{13}CHD_2$}-labeled methyls of ubiquitin at 25 and 5 °C, respectively, while the corresponding average R_1 values of 0.75 and 0.96 s^{-1} were obtained, respectively. Average ^{13}C R_2 and R_1 rates of 14.3 and 0.29 s^{-1}, respectively, were obtained for Ileδ1-{$^{13}CHD_2$} methyls of MSG, practically identical to the rates reported earlier.[9]

Data Analysis. Relaxation rates were extracted from fits of peak intensities to a single-exponential decay function, $A\exp(-RT)$, where R is the corresponding relaxation rate. R_2 values were calculated from $R_{1\rho}$ rates using the relationship, $R_2 = (R_{1\rho} - R_1\cos^2\lambda)/\sin^2\lambda$, where λ is the angle subtended by the direction of the effective spin-lock RF field with respect to the z-axis of the laboratory frame. In all calculations, $\theta_{axis,HH} = 90^o$, $\theta_{axis,CH} = 110.4^o$, and $r_{CH} = r_{CD} = 1.117$ Å were used for intra-methyl interactions,[12,13], along with $r_{HH} = \sqrt{3}\sin(\theta_{axis,CH})r_{CH} = 1.813$ Å, as in the previous studies of methyl axis dynamics by ^1H relaxation.[14] Methyl ^{13}C CSA (Δ_C) values of 25 ppm and 18 ppm was used for Leu/Val and Ile methyls, respectively.[15]

Eqs. S3-S4 were used in all calculations of relaxation rates for extraction of methyl axis dynamics parameters in this work, while Eqs. S5 form the basis for corrections applied to R_2/R_1 relaxation rates of the ($L_1 \pm L_4$) magnetization modes (see main text). Analysis of ^{13}C R_2/R_1 relaxation in $^{13}CHD_2$ methyl isotopomers closely followed that described previously[9] (see SI of ref. 9 for expressions describing R_2 and R_1 relaxation rates in $^{13}CHD_2$ methyls). Random errors in S^2_{axis} and τ_f values were estimated on the basis of 300 Monte-Carlo simulations,[16] and were on average 1.1 and 1.7 % for $^{13}CH_3$-derived S^2_{axis} in ubiquitin at 25 and 5 °C, respectively, while the corresponding errors for $^{13}CHD_2$-derived S^2_{axis} were 0.5 and 0.8 %, respectively. Random errors for $^{13}CH_3$-derived and $^{13}CHD_2$-derived S^2_{axis} in MSG (37 °C) were on average 2.5 and 1.8 %, respectively.

Supplementary References

1. Lipari, G.; Szabo, A. Model-Free Approach to the Interpretation of Nuclear Magnetic Relaxation in Macromolecules: 1. Theory and Range of Validity. *J. Am. Chem. Soc.* **1982**, *104*, 4546-4559.
2. Lipari, G.; Szabo, A. Model-Free Approach to the Interpretation of Nuclear Magnetic Relaxation in Macromolecules: 2. Analysis of Experimental Results. *J. Am. Chem. Soc.* **1982**, *104*, 4559-4570.
3. Skrynnikov, N. R.; Millet, O.; Kay, L. E. Deuterium Spin Probes of Side-Chain Dynamics in Proteins. 2. Spectral Density Mapping and Identification of Nanosecond Time-Scale Side-Chain Motions. *J. Am. Chem. Soc.* **2002**, *124*, 6449-6460.
4. Kay, L. E.; Bull, T. E. Heteronuclear Transverse Relaxation in AMX, AX_2, and AX_3 Spin Systems. *J. Magn. Reson.* **1992**, *99*, 615-622.
5. Tugarinov, V.; Karamanos, T. K.; Ceccon, A.; Clore, G. M. Optimized NMR Experiments for the Isolation of I=1/2 Manifold Transitions in Methyl Groups of Proteins. *Chemphyschem* **2020**, *21*, 13-19.
6. Ceccon, A.; Tugarinov, V.; Bax, A.; Clore, G. M. Global Dynamics and Exchange Kinetics of a Protein on the Surface of Nanoparticles Revealed by Relaxation-Based Solution NMR Spectroscopy. *J. Am. Chem. Soc.* **2016**, *138*, 5789-5792.
7. Tugarinov, V.; Kanelis, V.; Kay, L. E. Isotope Labeling Strategies for the Study of High-Molecular-Weight Proteins by Solution NMR Spectroscopy. *Nat. Protoc.* **2006**, *1*, 749-754.
8. Tugarinov, V.; Muhandiram, R.; Ayed, A.; Kay, L. E. Four-Dimensional NMR Spectroscopy of a 723-Residue Protein: Chemical Shift Assignments and Secondary Structure of Malate Synthase G. *J. Am. Chem. Soc.* **2002**, *124*, 10025-10035.
9. Tugarinov, V.; Kay, L. E. Quantitative 13C and 2H NMR Relaxation Studies of the 723-Residue Enzyme Malate Synthase G Reveal a Dynamic Binding Interface. *Biochemistry* **2005**, *44*, 15970-15977.
10. Tugarinov, V.; Ollerenshaw, J. E.; Kay, L. E. Probing Side-Chain Dynamics in High Molecular Weight Proteins by Deuterium NMR Spin Relaxation: An Application to an 82-Kda Enzyme. *J. Am. Chem. Soc.* **2005**, *127*, 8214-8225.
11. Delaglio, F.; Grzesiek, S.; Vuister, G. W.; Zhu, G.; Pfeifer, J.; Bax, A. Nmrpipe: A Multidimensional Spectral Processing System Based on Unix Pipes. *J. Biomol. NMR* **1995**, *6*, 277-293.

12. Ishima, R.; Petkova, A. P.; Louis, J. M.; Torchia, D. A. Comparison of Methyl Rotation Axis Order Parameters Derived from Model-Free Analyses of 2H and 13C Longitudinal and Transverse Relaxation Rates Measured in the Same. *J. Am. Chem. Soc.* **2001**, *123*, 6164-6171.

13. Ottiger, M.; Bax, A. How Tetrahedral Are Methyl Groups in Proteins? A Liquid Crystal NMR Study. *J. Am. Chem. Soc.* **1999**, *121*, 4690-4695.

14. Tugarinov, V.; Kay, L. E. Relaxation Rates of Degenerate 1H Transitions in Methyl Groups of Proteins as Reporters of Side-Chain Dynamics. *J. Am. Chem. Soc.* **2006**, *128*, 7299-7308.

15. Tugarinov, V.; Scheurer, C.; Brüschweiler, R.; Kay, L. E. Estimates of Methyl 13C and 1H CSA Values in Proteins from Cross-Correlated Spin Relaxation. *J. Biomol. NMR* **2004**, *30*, 397-406.

16. Kamith, U.; Shriver, J. W. Characterization of the Thermotropic State Changes in Myosin Subfragment-1 and Heavy Meromyosin by UV Difference Spectroscopy. *J. Biol. Chem.* **1989**, *264*, 5586-5592.